Spatial cell fate manipulation of human pluripotent stem cells by controlling the microenvironment using photocurable hydrogel

Zhe Wang[1,2], Akira Numada[1,2], Fumi Wagai[1], Yusuke Oda[1,2], Masatoshi Ohgushi[1,2], Koichiro Maki[3], Taiji Adachi[3] and Mototsugu Eiraku[1,2,4,*]

ABSTRACT

Human pluripotent stem cells (hPSCs) dynamically respond to their chemical and physical microenvironment, dictating their behavior. However, conventional *in vitro* studies predominantly employ plastic culture wares, which offer a simplified representation of the *in vivo* microenvironment. Emerging evidence underscores the pivotal role of mechanical and topological cues in hPSC differentiation and maintenance. In this study, we cultured hPSCs on hydrogel substrates with spatially controlled stiffness. The use of culture substrates that enable precise manipulation of spatial mechanical properties holds promise for better mimicking *in vivo* conditions and advancing tissue engineering techniques. We designed a photocurable polyethylene glycol-polyvinyl alcohol (PVA-PEG) hydrogel, allowing the spatial control of surface stiffness and geometry at a micrometer scale. This versatile hydrogel can be functionalized with various extracellular matrix proteins. Laminin 511-functionalized PVA-PEG gel effectively supports the growth and differentiation of hPSCs. Moreover, by spatially modulating the stiffness of the patterned gel, we achieved spatially selective cell differentiation, resulting in the generation of intricate patterned structures.

KEY WORDS: Hydrogel, Human pluripotent stem cell, Differentiation, Spatial control

INTRODUCTION

hPSCs are intensively used in regenerative medicine and developmental biology research. Many types of cells and tissues have been generated from hPSCs, providing a powerful tool for *in vitro* study. However, the current culture system is distinct from the *in vivo* microenvironment, limiting the generation of complex structures *in vitro*. Pluripotent stem cells (PSCs) can be cultured for differentiation in two- or three-dimensional (2D or 3D) conditions. 2D culture provides a simple, reproducible and robust culture condition, and many cell differentiation protocols have been developed in 2D. In contrast, in 3D culture, cells form aggregates that float in the culture medium or are embedded in an ECM (Gattazzo et al., 2014; Simunovic and Brivanlou, 2017). In both culture systems, stem cells are differentiated by adjusting the composition of the culture medium. 2D culture systems are subject to mechanical constraints on tissue shape because cells are cultured on a rigid culture dish. In contrast, in 3D culture systems, induced tissues are less mechanically constrained and can more freely change their shape. During development, stem cells organize into organs under relatively mild mechanical constraints through a combination of chemical and mechanical signals mediated by interactions between different tissues. (Simunovic and Brivanlou, 2017). Therefore, to induce functional tissues with appropriate shapes *in vitro*, an ideal environment allows tissue deformation with weak mechanical constraints.

Increasing evidence suggests the importance of mechanical cues on cell behavior and fate (Candiello et al., 2013; Chen et al., 2020; Keung et al., 2012; Maldonado et al., 2017; Muduli et al., 2017; Musah et al., 2014; Przybyla et al., 2016; Rosowski et al., 2015). Soft substrates and high mechanical tension enhance hPSC mesodermal differentiation (Muncie et al., 2020; Przybyla et al., 2016). Simultaneously, substrate geometry and structures are also crucial to complex tissue structure generation (Karzbrun et al., 2021; Warmflash et al., 2014). During development, neighboring cells communicate, sensing the surrounding chemical and mechanical cues, and differentiate accordingly. Eventually, stem cells gain differentiated cell fate and cooperate to form organs with complex structures. Therefore, it is important to spatially control the microenvironment to generate complex cellular structures. To this end, we aimed to develop a culture substrate with adjustable mechanical properties.

Hydrogels have been used intensively in biomedical research as cell culture substrates due to their mechanical and chemical similarity with the ECM (Tibbitt and Anseth, 2009). Furthermore, hydrogels can be functionalized with different properties, such as photocurability. Photocurable hydrogels based on hyaluronic acid and gelatin have been developed (Chen et al., 2019; Tibbitt and Anseth, 2009). By controlling the spatial pattern of illumination, gels with different shapes and structures can be generated. However, these gels were used for hPSCs encapsulation, but not for attachment due to poor adhesivity on the synthetic surface of hPSCs (Tibbitt and Anseth, 2009; Virdi and Pethe, 2021). In contrast, some hydrogels allow suitable hPSC attachment, such as polyacrylamide or polydimethylsiloxane (PDMS), that have been used intensively in studies regarding substrate stiffness (Chen et al., 2019; Chen et al., 2020; Maldonado et al., 2017; Millar-Haskell et al., 2019; Perez-Puyana et al., 2020; Tibbitt and Anseth, 2009). However, they lack flexibility in terms of gel structure and mechanical property control. Driven by this discussion, we developed a photocurable hydrogel with ideal hPSCs attachment.

[1]Laboratory of Developmental Systems, Institute for Life and Medical Sciences, Kyoto University, Kyoto 606-8507, Japan. [2]Department of Polymer Chemistry, Graduate School of Engineering, Kyoto University, Kyoto 606-8507, Japan. [3]Laboratory of Biomechanics, Institute for Life and Medical Sciences, Kyoto University, Kyoto 606-8507, Japan. [4]Institute for Advanced Study of Human Biology (WPI-ASHBi), Kyoto University, Yoshida-Konoe-Cho, Sakyo-Ku, Kyoto 606-8501, Japan.

*Author for correspondence (eiraku.mototsugu.2u@kyoto-u.ac.jp)

Z.W., 0000-0002-6717-0253; M.E., 0000-0002-9433-9085

DEVELOPMENT

hPSCs attach to the substrate via integrin-ECM protein interactions. Therefore, ECM protein engraftment on the hydrogel is necessary. Previously, ECM protein functionalized PVA could be used for hPSCs culture (Muduli et al., 2017). Polyvinyl alcohol (PVA), a polymer with a simple structure, can form a stable and biocompatible hydrogel upon cross-linking. We used PVA as the backbone and further functionalized PVA to have photocurability and ECM proteins to facilitate hPSCs attachment.

Here, we demonstrated a composite photocurable PVA and PEG hydrogel with adjustable stiffness and shape. Our hydrogel supports hPSC growth and differentiation, and the differentiation tendency of hPSCs was compared with cells cultured on plastic dishes. Most importantly, we demonstrated that stem cell fate could be spatially manipulated at a micrometer level by controlling the local mechanical property of substrates.

RESULTS

Synthesis and characterization of photocurable PVA-methacrylate hydrogel

To develop a photocurable hydrogel with protein binding ability, we used a denatured polyvinyl alcohol (PVA-COOH), which contains randomly integrated carboxyl groups as starting material. The carboxyl group in the PVA backbone can be activated by 1-ethyl-3-(3-dimethylaminopropyl) carbodiimide/N-hydroxysuccinimide (NHS/EDC) and further forms an amide bond with the N terminus of the ECM protein to enable cell attachment (Fig. 1A). To obtain photocurability, a methacrylate functional group was introduced into the PVA backbone to obtain photocurable PVA-MA. Lithium phenyl-2,4,6-trimethyl-benzoyl phosphonate (LAP) (0.5%) was used as the photoinitiator (Fig. 1B).

Increasing evidence suggests the importance of the diameter of colony and substrate geometry in generating complex tissue *in vitro* (Karzbrun et al., 2021; Warmflash et al., 2014). However, current micropatterned cultures are typically constructed on glass or plastic culture ware, and the mechanical properties of cellular substrates *in vitro* are very different from those under *in vivo* conditions. Taking advantage of the flexibility of photoinitiated crosslinkability of our hydrogel, we attempted to develop a patterned culture method using our hydrogel. As seen in Fig. 2C, we generated a spacer with a round hole in the center using PDMS. The spacer was then put on the glass-bottom dish. Hydrogel prefabrication solution was added into the hole and then covered by a coverslip. We then used a direct-exposure photolithography system to spatially control the illumination pattern to initiate gelation. With this method, we were able to create various-shaped gels at the micrometer level (Fig. 1C,D). However, we encountered an issue where the PVA-MA gel alone was too soft. Previous research demonstrated that by incorporating 4-arm PEG with different molecular weights and ratios, hydrogels with stiffness ranging from ∼500 Pa to 500 kPa could be obtained (Lee et al., 2014). Therefore, we introduced 4-arm PEG to create a composite hydrogel. We could also control the stiffness of the PVA-PEG composite hydrogel by adjusting the UV irradiation dosage. In this study, we used a mixture of 3% PVA and 15% 5 K 4-arm PEG, as it provided us with a soft, *in vivo*-like stiffness and clear boundaries when generating gel patterns (Fig. 1D,E). Consequently, we have developed a photocurable hydrogel substrate with adjustable stiffness, ranging from soft (∼700 Pa) to hard (∼6 kPa), achieved through the combination of 3% PVA and 15% 5k 4-arm PEG.

The crosslink density not only influences the stiffness of the hydrogel but also the mesh size of the hydrogel network. This can potentially impact cells by affecting the diffusion of proteins in the culture medium. Therefore, we investigated the diffusivity of fluorescent molecules with varying molecular weights in gels with different stiffness levels.

As illustrated in Fig. 1F and Fig. S1, molecules with a molecular weight of 4 kDa or larger were unable to diffuse within both hard and soft hydrogels. However, when using a molecule with a molecular weight of 1.4 kDa, it was capable of diffusing into both hard and soft gels, with the soft gel exhibiting higher diffusivity.

To assess the protein-binding capability of PVA-MA, we incubated both activated and non-activated PVA-MA with a fluorescent protein (Fig. 1G). After incubation, we measured the fluorescence intensity to quantify the protein-binding capacity of the hydrogel. The activated gel exhibited a significantly higher fluorescent signal (Fig. 1H), ∼20 times that of the non-activated hydrogel and ∼2.2 times that achieved with conventional coating methods on a glass surface. This result indicates successful protein binding to our hydrogel.

PVA-PEG gels support hPSC survival and outgrowth while maintaining pluripotency

Next, we tested whether our gel supports hPSC growth. We generated two types of gels: one with a stiffness of ∼6 kPa (hard) and another with a stiffness of around 700 Pa (soft). These gels were then activated and coated with laminin 511 as ECM proteins for hPSC culture.

To analyze cell proliferation, we developed a nucleus reporter H2B-mCherry hPSCs line that enabled us to track cell movements and conduct cell cycle analysis. H2B-mCherry-labeled cells were seeded on culture dishes or hydrogels, and live imaging was performed to monitor cell nuclear division. We found that cells cultured on the gel exhibited a similar proliferation rate compared with those cultured on glass-bottom dishes (Fig. 2A). Cells on the softer gel displayed slightly longer cell cycles, consistent with previous reports (Guo et al., 2020; Shao et al., 2015).

Immunofluorescence (IF) analysis indicated that hPSCs cultured on both hard and soft hydrogels maintained their pluripotency within one passage. This was evidenced by the expression of pluripotent markers (SOX2, OCT4 and NANOG) in day 6 cultures on the gel (Fig. 2B). These results suggest that pluripotency and proliferation of hPSCs can be sustained on hydrogels, at least within the observed time window (6 days).

It was previously known that hPSCs tend to lose nuclear-localized YAP when cultured on relatively soft substrates, a key mechano-reactive gene involved in various biological processes. Therefore, we investigated the impact of our gel on YAP localization. Cells on hard gel and conventional glass dishes exhibited clear nuclear-localized YAP, whereas cells on the soft gel did not (Fig. 2C, Fig. S3A,B). The hard gel exhibited lower nuclear-localized YAP than the dish (Fig. S3B). This nuclear-localized YAP can be downregulated by the Rho-kinase inhibitor Y-27632 (Fig. S3A,B). Interestingly, cells on the hard gel also displayed nuclear YAP, even though it was shown that hPSCs lost nuclear YAP on a substrate with similar stiffness (Estaras et al., 2017; Pagliari et al., 2021; Qin et al., 2016; Stronati et al., 2022). The difference from our observations is likely due to the high protein binding capacity of our gel (∼2.2 times of glass surface), which results in a dense ECM ligand (Fig. 1G,H), thus promoting nuclear YAP, as observed previously (Kechagia et al., 2023; Lee et al., 2019; Stanton et al., 2019).

Comparative analysis of hPSCs cultured on hydrogel and glass substrates by RNA-sequencing

We assessed the impact of substrate stiffness on hPSCs gene expression. On day 4, hPSCs cultures on hard gel (∼6 kPa), soft gel
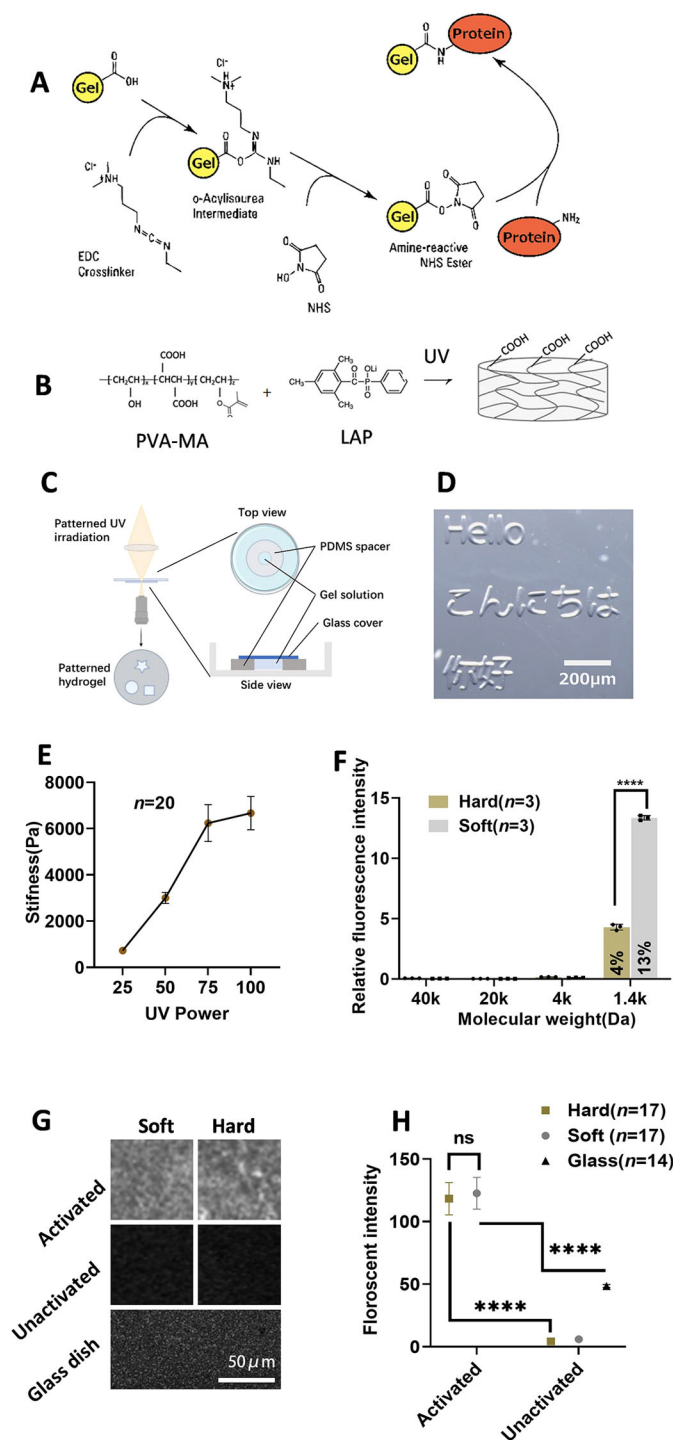
DEVELOPMENT

Fig. 1. Photocurable PVA-PEG hydrogel. (A) The hydrogel can be activated to bond with proteins using 1-ethyl-3-(3-dimethylaminopropyl) carbodiimide/N-hydroxysuccinimide (NHS/EDC). (B) PVA-MA forms COOH-containing hydrogel upon ultraviolet (UV) irradiation. (C) Schematic for generating patterned hydrogel. (D) Patterned gel was generated using patterned UV irradiation, as shown in C. (E) Stiffness measurements for hydrogel generated using different UV doses. Data are mean±s.d. (*n*=20). (F) Fluorescent diffusion experiment: hydrogels were incubated with fluorescent molecules. Data are mean fluorescent intensity inside the gel relative to incubation solution±s.d. Black dots represent each sample (*n*=3). (G) Fluorescent protein-binding experiments. Activated and non-activated soft and hard gels, together with a glass-bottom dish, were incubated with fluorescent protein to evaluate the protein-binding ability. (H) Quantification of fluorescent protein binding experiments. Fluorescence intensity was measured using fluorescence microscopy (*n*=17 for hard, *n*=17 for soft, *n*=14 for glass). Data were obtained from at least three biological replicates. Data are mean±s.d. with the median values indicated by black horizontal lines. Scale bars: 200 μm in D; 100 μm in G. ns, not significant. ****$P<0.0001$(unpaired two-tailed *t*-test).

gel (Fig. 3D). Compared with culture dishes, gene ontology (GO) analysis indicated that soft hydrogels were enriched with genes related to: 'formation of the beta-catenin:TCF transactivating complex', 'cell morphogenesis', 'endoderm development' and 'degradation of the extracellular matrix' (Fig. S2A). Hard gel enriched gene groups are: 'cell morphogenesis involved in differentiation', 'endoderm development' and 'tissue morphogenesis' (Fig. S2B). Additionally, the hard gel displayed a significantly higher expression of YAP downstream genes than the soft gel, consistent with our immunofluorescence results (Fig. 2C, Fig. S2C).

Previous reports have shown that culturing hPSCs on a 3 kPa substrate upregulates the long noncoding RNA (lncRNA) LINC00458 and LINC01356, and LINC00458 interacts with SMAD 2/3, a downstream effector of Nodal, thereby promoting endoderm differentiation (Chen et al., 2020). We noticed that these genes were also upregulated in cells cultured on the soft and hard gels (Fig. S2D).

In summary, hPSCs cultured on both soft and hard gels exhibited upregulated NODAL-related genes, possibly mediated by LINC00458 and SMAD2/3 upregulation. Cells on the hard gel expressed higher YAP downstream genes and slightly higher but not significantly different endoderm-related genes, likely due to the preferred stiffness range for endoderm differentiation (Chen et al., 2020; Maldonado et al., 2017; Srivastava et al., 2023). Notably, both the hard and soft gels maintained pluripotency within the observed time window, as evidenced by pluripotent gene expression (Fig. 3C).

hPSCs can be differentiated into all germ layers on PVA-PEG gel

Given the fact that our gel with different stiffness levels has varying impact on the transcriptome, we next evaluated whether it could be used for differentiation towards three germ layers. Cells passaged on the PS dish were collected and seeded on the hard PVA-PEG gel, and subsequently differentiated towards three germ layers following previously reported protocols (D'Amour et al., 2005; Evseenko et al., 2010; Loh et al., 2016; Surmacz et al., 2012).

For neural ectoderm (NE), hPSCs were differentiated using the previously reported dual SMAD inhibition method (Chambers et al., 2009). After 6 days of differentiation, cells on both polystyrene (PS) dish and hydrogels largely expressed the NE markers, PAX6 and OTX2, suggesting successful NE differentiation (Fig. 4A,B, Fig. S4). qPCR results indicate that

(~700 Pa) and glass-bottom dishes were collected for RNA-seq analysis. Notably, pluripotent genes such as SOX2, OCT3/4 and NANOG showed similar expressions in all samples (Fig. 3C), consistent with immunostaining results (Fig. 2C). We next identified differentially expressed genes (DEGs) among each sample. As a result, we found that NODAL-related genes such as *NODAL*, *ANXA1*, *CER1*, *FOXA2*, *LEFTY1*, *LEFTY2*, *SMAD7*, *SERPINE1* and *TIMP4* were upregulated in both soft and hard gels compared with culture dishes (Fig. 3D). The hard gel exhibited slightly higher endoderm gene expression compared with the soft
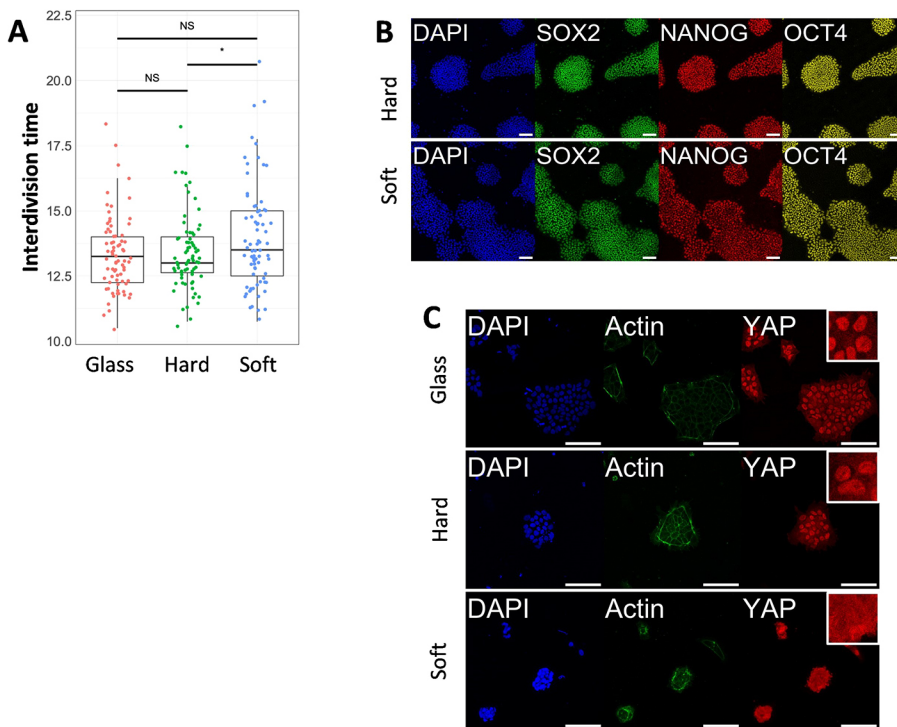
Fig. 2. Human pluripotent stem cell proliferation and YAP localization.
(A) Interdivision time of human pluripotent stem cells (hPSCs) cultured on hard gel, soft gel and conventional glass culture dishes. Dots represent results from individual cells (n=75). The box plot illustrates the interquartile range (from Q1 to Q3) with a median line, while the whiskers extend to the most extreme value that is not labeled as an outlier. (B) Immunofluorescent staining of pluripotent markers in day 6 cells cultured on soft and hard gels. (C) Immunofluorescent staining of YAP in hPSCs cultured on gels and conventional glass dishes. White boxes indicate 40×40 µm area magnifications of YAP staining. Data were obtained from at least three biological replicates. Scale bars: 100 µm. ns, not significant. *P<0.1 (unpaired two-tailed t-test).

cells differentiated on culture dishes showed similar NE gene expression as cells differentiated on hard and soft gels. This is consistent with a previous report comparing NE differentiation on hydrogels (700 Pa, 75 kPa and 300 kPa) and culture dishes (2.28-3.28 GPa). (Fig. 4B) (Keung et al., 2012; Maldonado et al., 2017).

For definitive endoderm (DE), cells were first differentiated to the anterior primitive streak (APS) for 24 h and then towards DE (D'Amour et al., 2005; Evseenko et al., 2010). As Fig. 4C shows, cells on both culture dishes and gels were successfully differentiated, supported by expression of the NE marker SOX17 in most cells (Fig. S4). Interestingly, qPCR revealed a notably enhanced expression of APS and DE-related genes on hard and soft gels compared with the culture dish. However, there is no statistically significant difference between soft and hard gel (Fig. 4D).

For mesodermal development, the paraxial mesoderm (PM) and lateral plate mesoderm (LPM) fates separate at the early stages of differentiation; therefore, we tested both. For LPM, hESCs cells were differentiated toward mid primitive streak (MPS) for 24 h and then towards LPM for 24 h following the previously reported protocol (Loh et al., 2016). Immunostaining results suggested that the differentiation both on the gel and culture dish was successful (Fig. 4E, Fig. S4). Cells differentiated on gels expressed a higher level of *HAND1* and *ISL1* but expressed a lower level of *NKX2.5* (Fig. 4F).

For PM, hPSCs were differentiated towards APS for 24 h, and then APS was directed towards PM for 24 h (Loh et al., 2016). Although soft substrate has previously been shown to enhance mesendoderm fate (Chen et al., 2020; Przybyla et al., 2016), immunofluorescence and qPCR reflected similar expression of LPM markers in our experiments (Fig. 4G, Fig. S4). These results indicate that hPSCs on our hydrogels can be successfully differentiated to NE, DE, LPM and PM, as they can on PS substrates (Fig. S4).

Soft substrates have been shown to enhance mesendoderm differentiation (Pagliari et al., 2021; Przybyla et al., 2016). However, for both PM and LPM, qPCR revealed different differentiation efficiencies on the gel compared with conventional dishes, yet the changes remained within a similar range (less than a twofold change). We hypothesized that the extended differentiation processes of PM and LPM, involving multiple steps (APS to PM or MPS to LPM), could mitigate the impact of the substrate on mesoderm differentiation. Therefore, we next differentiated hPSCs into the early mesendoderm (primitive streak) population using BMP4, as previously reported (Evseenko et al., 2010; Przybyla et al., 2016). Indeed, when compared with a conventional dish, the early mesoderm markers T and MESP1 showed a 6- and 10-fold upregulation on hard gel compared with glass dish (Fig. 4I).

Mesodermal differentiation was shown to be affected by cell density (Kempf et al., 2016; Smith et al., 2018). To avoid the effects caused by unequal distribution of cell numbers in colonies, we next decided to use patterned culture, creating a homogeneous condition to mitigate the impact of colony size on differentiation efficiency.

Manipulating cell fate of hPSCs on the patterned gel by controlling substrate stiffness

To examine how stiffness affects stem cell fate when differentiated to early mesendoderm (primitive streak), we first generated soft and hard patterned gels, and differentiated hPSCs on gels towards the mesendoderm by administrating 10 ng/ml BMP4 and bFGF (Evseenko et al., 2010; Przybyla et al., 2016) in differentiating medium (Fig. S5A). After 24 h of differentiation, cells on the soft gel were differentiated to a mesendoderm fate that was indicated by the expression of mesendodermal and primitive streak marker T. Most cells on hard gels do not express T, except a few cells on the edge (Fig. S5B), probably due to weaker cell-cell junction and higher tension (Muncie et al., 2020; Przybyla et al., 2016). These results indicate that it is possible to manipulate stem cell fate by adjusting the stiffness of the hydrogel. As the stiffness of the gel is
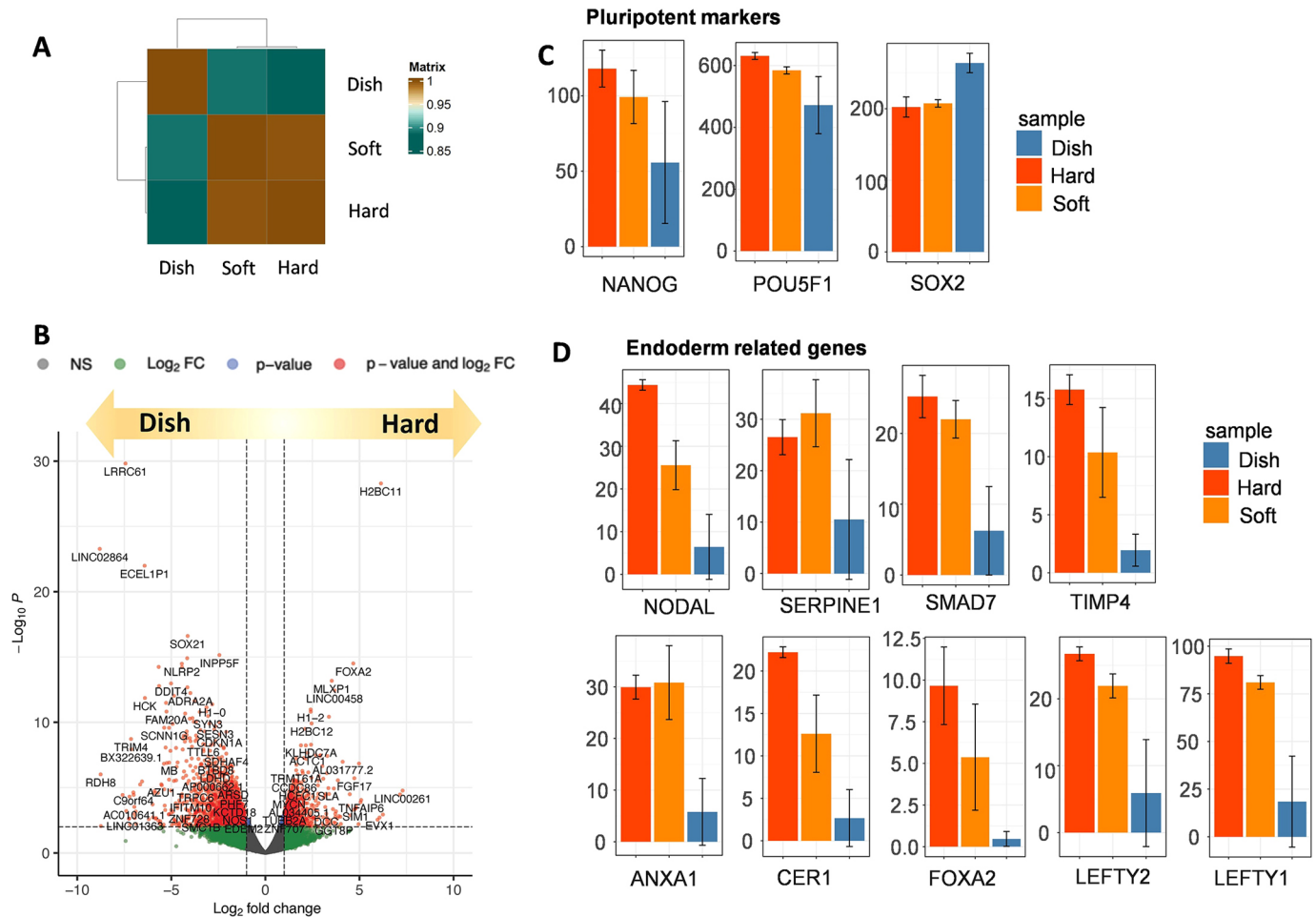
Fig. 3. Transcriptome analysis of human pluripotent stem cells cultured on soft or hard gel, or in a conventional glass dish. (A) Hierarchical clustering analysis of mRNA expression in human pluripotent stem cells (hPSCs) cultured on soft and hard substrates compared with conventional glass dishes (n=2). The figure displays the mean value of the two samples. (B) A volcano plot representing the entire gene expression dataset for hPSCs cultured on a soft gel versus dish for 4 days. Red color indicates differentially expressed genes; dots represent individual genes. Insignificant genes are in gray. (C) Expression levels of selected genes based on RNA-seq of hPSCs cultured on soft or hard gels, or in a conventional glass dish. Expression level is shown as transcripts per kilobase million (TPM). (D) Endoderm-related gene expression based on RNA-seq of hPSCs cultured on soft or hard gel, or in a conventional glass dish. Expression level is shown as TPM. Data are mean±s.d.

easily controlled by UV dosage, we next generated a hydrogel with locally different stiffness to investigate the possibility of spatially controlling stem cell fate (Fig. 5A, Fig. S5C). We created a hydrogel with locally varying stiffness and confirmed the stiffness distribution in the gel pattern, which revealed a clear boundary between soft and hard areas (Fig. 5A,B).

We seeded hPSCs on a patterned hydrogel, with one half being hard and the other half soft. After 24 h of differentiation towards early mesendoderm, cells in the hard areas remained pluripotent, as indicated by positive SOX2 and negative T expression. Conversely, cells in the softer areas exhibited mesendodermal fate, as shown by their T expression and the absence of SOX2 expression (Fig. S5C). We calculated the number of T^+ cells per area based on the immunofluorescent image, as demonstrated in Fig. S5D, and found that cells on the softer gel pattern had a significantly higher (~200 times) rate of T^+ cells. Fig. S5E illustrates the distribution of T^+ cells per area in both soft and hard areas.

Despite the significant difference in T^+ cell number after 24 h of differentiation, we found that cells on both the hard and soft areas became T^+ after 48 h differentiation in the presence of BMP4 and bFGF. Therefore, we next tested whether it is possible to maintain

the patterned differentiation by administering a pulse of morphogen stimulation. hPSCs were seeded on hydrogel patterns and cultured in the pluripotency maintenance medium. BMP4 and bFGF (10 ng/ml each) were directly added into the maintenance medium for 24 h and then withdrawn by medium change (Fig. 5C). The cells were cultured in a maintenance medium for another 48 h. As shown in Fig. 5D, cells on the soft gel predominantly express T markers, whereas few or no T^+ cells are observed on hard gels. Notably, on patterned gels, T^+ cells are primarily localized in the soft areas, and these cells exhibit a loss of SOX2 expression, as shown in Fig. 5E,F. These data suggest that we could selectively control cell differentiation by spatially controlling the hydrogel stiffness.

We next investigated how soft gels promote early mesoderm differentiation. During gastrulation, BMP4 triggers downstream Wnt signaling, inducing primitive streak formation (Martyn et al., 2018). RNA-seq analysis also implies that enhanced β-catenin formation on the soft gel substrate (Fig. S2A), a key component of the Wnt signaling pathway. This aligns with an earlier study (Przybyla et al., 2016) where cells cultured on a softer (400 Pa) gel exhibited stable adherens junctions, increased β-catenin accumulation and inhibited β-catenin degradation. Conversely,
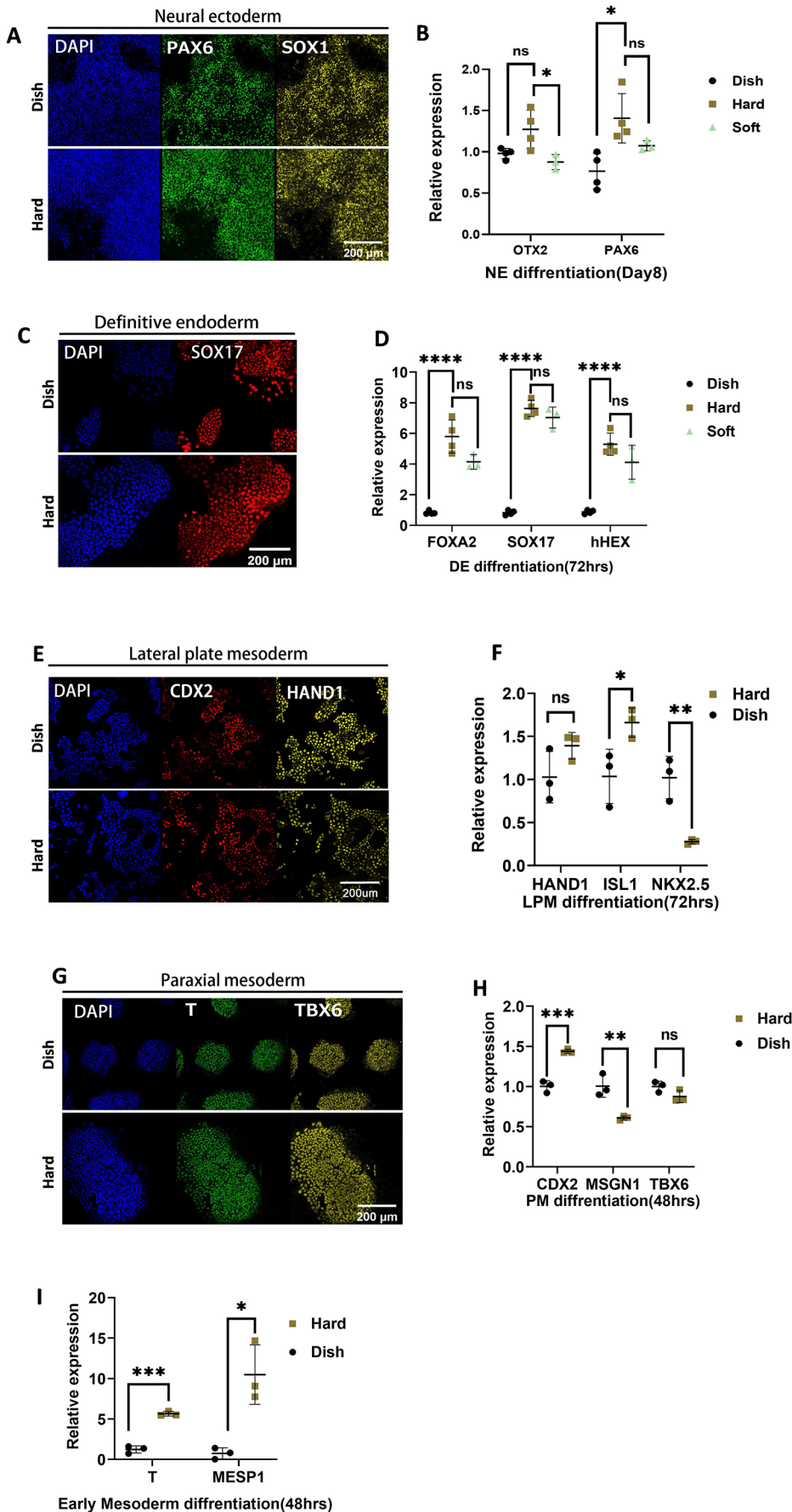
5

Fig. 4. Differentiation of human pluripotent stem cells on gel. (A) Immunofluorescence of neural ectoderm differentiation. (B) qPCR of neural ectoderm differentiation. (C) Immunofluorescence of definitive endoderm. (D) qPCR of definitive endoderm differentiation. (E) Immunofluorescence of lateral plate mesoderm. (F) qPCR of lateral plate mesoderm differentiation. (G) Immunofluorescence of paraxial mesoderm. (H) qPCR of paraxial mesoderm differentiation. (H) qPCR of early mesoderm (BMP/bFGF) differentiation. Scale bars: 200 μm. Data were obtained from at least three biological replicates. Each dot represents an individual biological replicate, with black lines indicating median values. Data are mean±s.d. Statistical significance was determined using an unpaired two-tailed *t*-test. ns, not significant. ****P<0.0001, ***P<0.001, **P<0.01, *P<0.1.
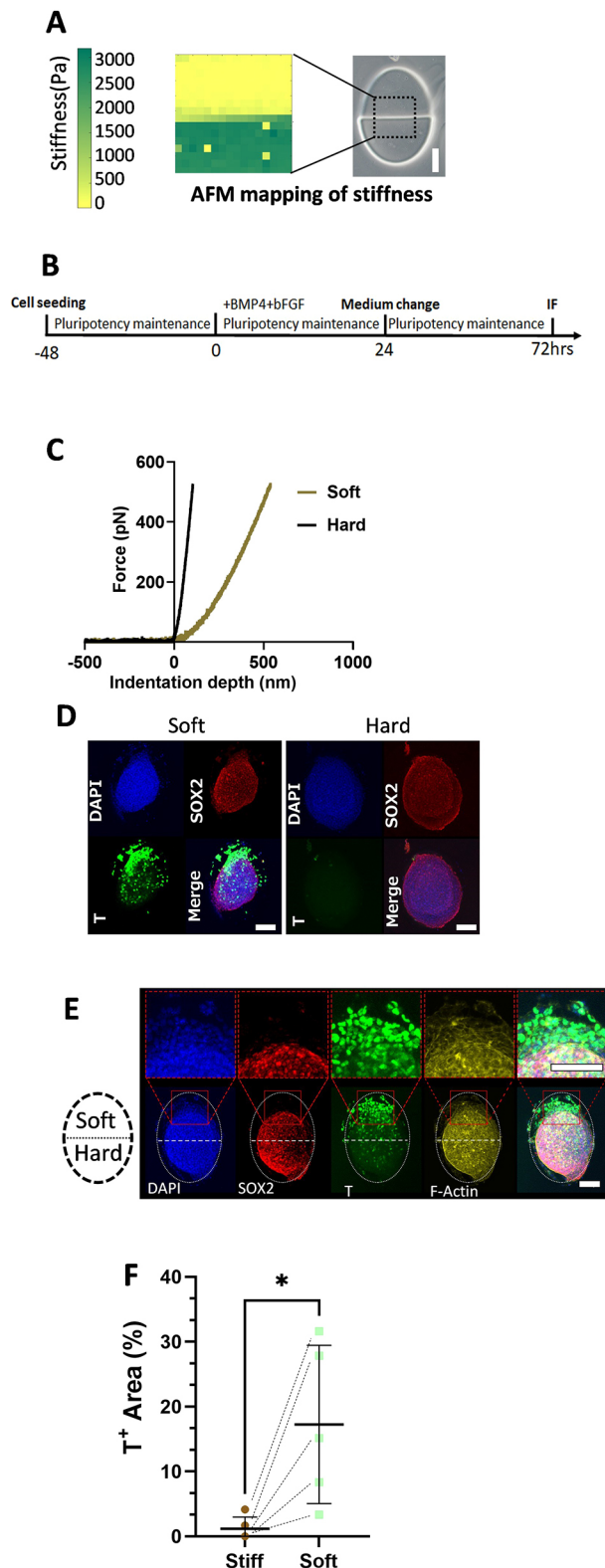
Fig. 5. Spatial control of hydrogel stiffness and stem cell fate.
(A) Presentation of patterned gel and a heatmap illustrating the surface stiffness of the gel measured using an atomic force microscope (AFM). The dotted outline indicates the region of the hydrogel pattern measured. (B) A schematic illustration depicting the differentiation method. (C) Representative AFM force curve data for soft and hard regions. The x-axis represents indentation depth (nm); the y-axis represents force (pN). (D) Immunofluorescent staining of cells differentiated on soft and hard gels using the method shown in C. (E) Immunofluorescent staining of cells differentiated on a partially soft gel using the method shown in C. The white dotted oval outlines the whole gel pattern, with the upper half being soft and the lower half being hard. Red squares contain magnified views of the indicated regions. Scale bars: 100 μm. (F) Quantification of immunofluorescence for cells differentiated on partially soft gel using pulse differentiation. Data are represented by T$^+$ area/gel surface area using maximum projection of immunofluorescent images. Dashed line-connected dots represent soft and hard parts from the same patterned gel. Data were obtained from at least three biological replicates. Black horizontal lines represent median values±s.d. *P<0.05 (one-tailed paired t-test).

cells on locally soft and hard gel patterns with BMP and bFGF in the presence of 2.5 μM IWP2, an inhibitor of Wnt secretion. This completely abolished differentiation, even when extended for 48 h (Fig. 6A).

Conversely, differentiation occurred in both hard and soft areas when we employed the GSK3 inhibitor CHIR99201 to inhibit β-catenin degradation. This differentiation occurred without a significant time difference between soft and hard regions, unlike when differentiated with BMP (Fig. 6A,B, Fig. S6A-C, Movie 1). These results suggest that downstream Wnt/β-catenin signaling is intimately involved in the different stem cell fates induced by BMP4 and FGF2 observed on hydrogels with different stiffness patterns.

As shown above, we observed a downregulation of YAP nuclear trafficking on softer gels (Fig. 2C). YAP serves as a major mechano-responsive gene and has been shown to influence hESCs differentiation into various germ layers, including mesoderm. Numerous studies have reported that YAP signaling activation has a negative impact on SMAD2/3 and Wnt signaling, thereby negatively regulating mesoderm differentiation (Estaras et al., 2017; Pagliari et al., 2021; Qin et al., 2016; Srivastava et al., 2023; Stronati et al., 2022). Conversely, inhibiting YAP nuclear trafficking promotes Wnt signaling and triggers gastrulation-like differentiation (Srivastava et al., 2023). Therefore, we next investigated the YAP and β-catenin expression before differentiation. As shown in Fig. 6E, on the hard part of the patterned gel, YAP still exhibited visible nuclear localization, whereas cells on the soft part displayed the opposite pattern (Fig. 6C). This aligns with the results we obtained on the non-patterned gel (Fig. 2C). Similarly, soft gel also showed stronger β-catenin staining (Fig. 2C), consistent with previous reports, a 400 Pa substrate promoted β-catenin accumulation and downregulated degradation (Przybyla et al., 2016). When differentiated with BMP4 and bFGF, this difference in β-catenin expression was still maintained (Fig. S7A,B). However, when β-catenin degradation was inhibited using the GSK3 inhibitor CHIR99201, the differences in β-catenin expression between the soft and hard regions, as well as the expression differences of T, were abolished (Fig. S7C,D). We next investigated whether the difference in stem cell fate could be abolished by inhibiting YAP signaling. T-tdTomato reporter cells on soft/hard patterned gel were pre-treated with 50 nM YAP-TEAD inhibitor 1 (Peptide 17) for 6 h and further differentiated in the presence of Peptide 17. Live imaging revealed that this inhibition of YAP also abolished the expression differences of T in the hard and soft regions (Fig. 6B,

β-catenin was destabilized and degraded in cells on a harder (60 kPa) gel. Consequently, cells on the softer gel exhibited heightened Wnt signaling sensitivity to BMP4-induced differentiation. To investigate the role of Wnt/β-catenin signaling, we conducted perturbation experiments. Initially, we differentiated
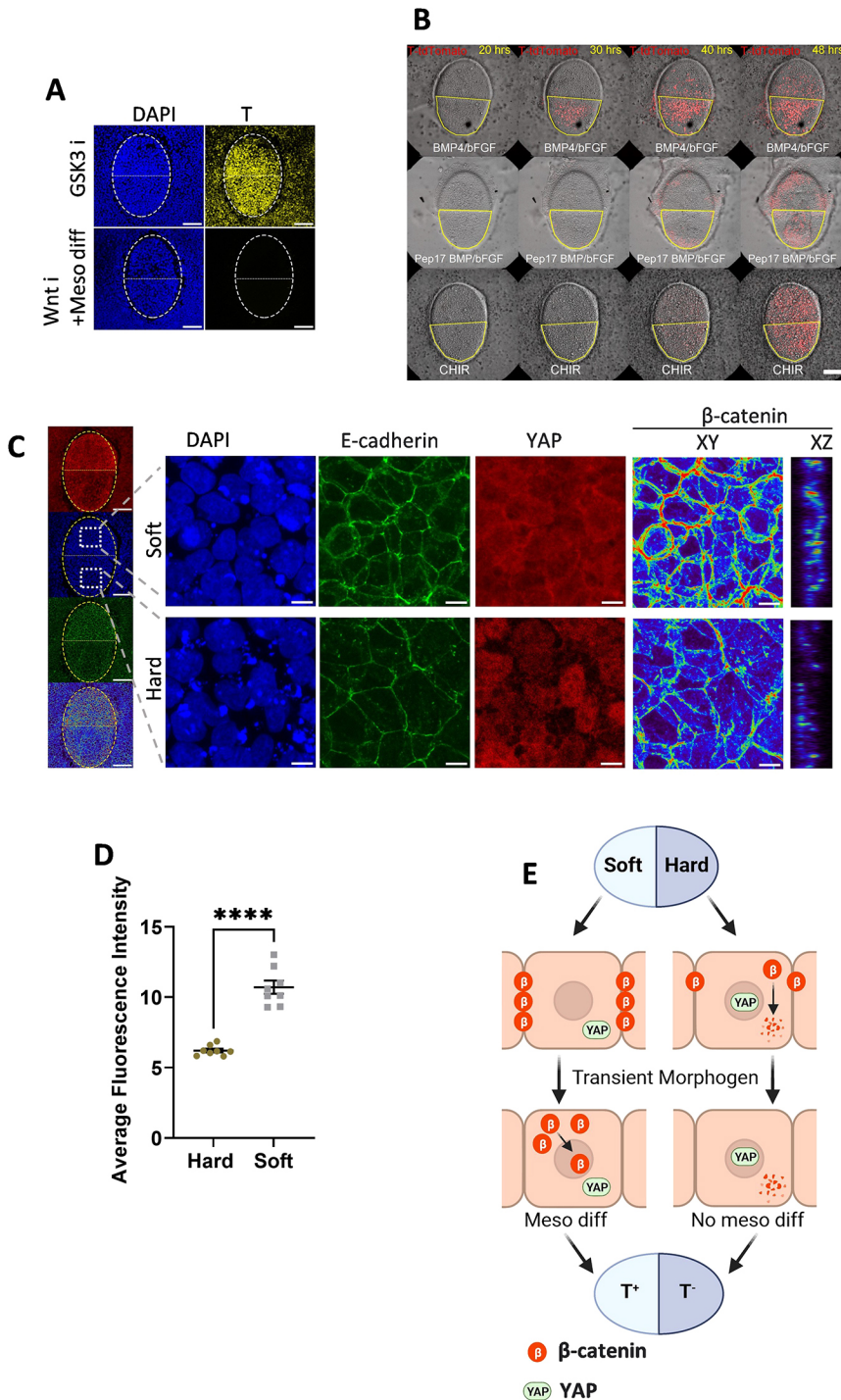
Fig. 6. Speculated mechanisms of stem cell fate control. (A) Immunofluorescent staining of cells differentiated using GSK3 inhibition or by BMP/bFGF together with Wnt inhibition on a partially soft gel. The white dotted oval line indicates the whole gel pattern, with the upper half being soft and the lower half being hard. Scale bars: 100 μm. (B) Screenshot of live imaging of T-tdTomato reporter cells differentiated on a patterned gel using BMP/bFGF with CHIR (Movie 1) and using BMP/bFGF in the presence of Peptide 17 (Movie 2). The red color represents the tdTomato signal. The yellow line circles the soft part of the gel. Scale bar: 100 μm. (C) Immunofluorescent staining of hPSCs on a partially soft gel pattern before differentiation. The yellow dotted oval line indicates the whole gel pattern, with the upper half being soft and the lower half being hard. The white squares indicate the positions of the magnified views. The β-catenin channel is shown in XY and XZ section views as a heat map, with colors representing fluorescent intensity. Scale bars: 100 μm in the whole gel view; 10 μm in the magnified view. (D) Quantification of β-catenin fluorescent intensity based on z sections of immunofluorescent staining of the soft and hard regions on the same gel pattern. Each dot represents an individual measurement ($n=8$). Data were obtained from at least three biological replicates. Data are mean±s.d. ****$P<0.0001$ (unpaired two-tailed t-test). (E) Proposed mechanism of spatial cell fate control. On the soft gel, β-catenin formation is enhanced and YAP nuclear localization is inhibited, promoting sensitivity to Wnt signaling. On the hard region, cells have nuclear-localized YAP, which negatively impacts Wnt signaling. Together with downregulated β-catenin compared with the soft part, this leads to decreased mesoderm differentiation compared with the soft region.

Movie 2). Our results suggest that the spatial difference in stem cell fate, manipulated by local stiffness, is likely mediated by YAP and Wnt/β-catenin signaling. In the hard region, nuclear-localized YAP and decreased β-catenin negatively affect Wnt signaling. In contrast, in the soft region, decreased YAP nuclear trafficking and upregulated β-catenin enhance sensitivity to Wnt stimulation, resulting in spatially distinct cell fates (Fig. 6E).

DISCUSSION

We developed a photocurable hydrogel for hPSCs culture. We have also shown that spatially patterned illumination of UV light using a digital mirror device could control the shape and the local stiffness of the patterned hydrogels. Laminin511 E8 fragment functionalized hydrogel supports hPSCs growth and maintenance of hPSC pluripotency. hPSCs can be differentiated towards all three germ layers on our developed hydrogel. We also demonstrated when cultured on the gel, NODAL-related genes are upregulated compared with PS dishes. Most importantly, by generating locally soft gels, we could selectively differentiate hPSCs towards the mesendodermal lineage and manipulate stem cell fate spatially.

To overcome the limitation of traditional 2D and 3D cultures, many soft substrates have been developed for cell cultures, such as

various hydrogels, electro-spun fibers and PDMS. However, owing to the poor adhesivity of hPSCs on the synthetic surface (Tibbitt and Anseth, 2009; Virdi and Pethe, 2021), only limited materials can be used for attachment culture. PA has been used for hPSCs attachment culture; however, the pluripotency cannot be maintained. Here, Laminin 511 E8 was covalently bonded to our hydrogel and provided a strong attachment for hPSCs to enable an ideal culture of hPSCs while maintaining pluripotency.

Soft substrates such as PVA, electro-spun fibers, PA gel and PDMS have previously been used for hPSCs attachment culture (Chen et al., 2020; Hsu et al., 2018; Keung et al., 2012; Kumbar et al., 2008; Muduli et al., 2017; Muncie et al., 2020; Musah et al., 2014; Pagliari et al., 2021; Przybyla et al., 2016; Virdi and Pethe, 2021). However, these methods usually coat the whole surface of the culture dish, and the local mechanical property cannot be adjusted. Recent research suggests the importance of the stiffness and geometry constraint in differentiating complex structures (Chen et al., 2020; Karzbrun et al., 2021; Keung et al., 2012; Martyn et al., 2018; Muncie et al., 2020; Musah et al., 2014; Przybyla et al., 2016; Rosowski et al., 2015; Srivastava et al., 2023; Virdi and Pethe, 2021). Our hydrogel provided a simple and flexible platform for generating a geometry- and local stiffness-defined culture substrate.

Currently, most of the differentiation protocols are developed by adjusting the culture medium composition. However, organs are an organized structure of different lineages. Differentiation of different lineages in a homogenous culture system by only adjusting medium composition is challenging. Here, we selectively differentiate hPSCs towards the mesendoderm by adjusting local stiffness; this provided a new tool for generating complex structures and contributing to regenerative medicine and tissue engineering.

The mechanical microenvironment plays a crucial role in stem cell fate determination. We noticed that when differentiating hPSCs on different stiffness substrates, the expression changes of marker genes do not appear linear with stiffness (Maldonado et al., 2017; Musah et al., 2014). It has been previously reported that in the range of 3 kPa to 1 GPa, the expression of APS and mesendoderm genes (EOMES and T) and DE genes (FOXA2 and SOX17) are inversely proportional to the substrate stiffness, but a soft substrate seems to inhibit the pan primitive streak gene *CDX2*, and the mesodermal genes FOXC2 and NKX2.5 (Chen et al., 2020). Substrate stiffness also affects the cell fate decision developmental stage specifically. PM-related genes remained at similar expression levels in our experiment and could be explained by different observed markers, time points and stiffness range.

Furthermore, even for a similar stiffness range, studies using different materials, such as electrospun nanofibers, have different results from those using hydrogels (Chen et al., 2020; Maldonado et al., 2017; Przybyla et al., 2016), indicating the culture substrate might not only affect cells by mechanotransduction but also other factors such as the substrate dimensionality and surface chemistry. The type and distribution of ECM proteins have been shown to influence stem cell mechanosensation and fate in conjunction with substrate stiffness (Kechagia et al., 2023; Lee et al., 2019; Shibata et al., 2018; Stanton et al., 2019; Wang et al., 2015; Zhang et al., 2017). In our research, to provide stable cell attachment, we used a high density of laminin 511, known for its strong cell attachment properties. Previous reports have indicated that the high density of ECM ligands on culture substrate promotes YAP nuclear trafficking. Our gel also exhibits a higher protein binding capacity compared with commercial glass dishes (Fig. 1G,H), resulting in a denser ligand density. This might explain why stem cells exhibited nuclear-localized YAP when cultured on our hard gel (6 kPa).

The interplay between ECM proteins and stiffness warrants further examination in future research.

We also found that endoderm gene expression was promoted on our gel, as indicated by our RNA-seq results (Fig. 3D), consistent with previous reports (Guo et al., 2020; Keung et al., 2012). Our developed hydrogel model promotes DE differentiation, likely through the upregulation of NODAL signaling mediated by LINC00458 and SMAD2/3 upregulation, as shown previously (Guo et al., 2020; Keung et al., 2012).

The mechanism for how our hydrogel, with other substrates, affects stem cell behavior is an important aspect to explore. Most studies discussing substrate stiffness used hydrogels (Chen et al., 2020; Keung et al., 2012; Maldonado et al., 2017; Muduli et al., 2017; Muncie et al., 2020; Pagliari et al., 2021; Przybyla et al., 2016; Virdi and Pethe, 2021). Hydrogels are polymer networks containing water molecules within these networks. Changing the number of crosslinks also changes the mesh size and surface chemistry, thus affecting the diffusion of the soluble factors at the basal side of the cell. In our research, we have shown that our gel can only allow small soluble factors (1.4 kDa) to penetrate but not those molecules that are bigger than 4 kDa, suggesting that the stem cell fate manipulation is not caused by differences of diffusible proteins such as those of TGFβ.

We have shown YAP nuclear trafficking downregulation and β-catenin upregulation on softer gels. Our gel enables spatial manipulation of YAP and Wnt/β-catenin signaling for stem cell fate control in the mesendoderm differentiation. Exploring the crosstalk between YAP and Wnt/β-catenin pathways, including their hierarchy, might be a focus for future research.

In summary, we have developed a novel method for the fabrication of hPSCs culture substrate. Taking advantage of the flexibility of gel geometry and stiffness, we could precisely control the geometry and spatial stiffness. By adjusting the stiffness locally, we could selectively differentiate hPSCs toward the mesoderm, providing a novel method to generate more complex tissue structures *in vitro*.

MATERIALS AND METHODS
Synthesis and preparation of hydrogel prefabrication solution
PVA (AP-17, Japan Vinyl Acetate & Poval; Mn=80,000-90,000) was reconstituted into a 5% PVA solution by slowly adding PVA into 50-60°C H_2O while stirring. The temperature was then increased to 90°C while stirring for 60 min for PVA to completely dissolve. The solution was subsequently cooled to 50°C while stirring. Sulfuric acid (400 µl) was added to the PVA solution dropwise while the temperature was maintained at ~50°C. Methacrylic anhydride (1.5 ml) (276685, Sigma-Aldrich) was added to the mixture dropwise while stirring until the mixture became cloudy. More sulfuric acid was added dropwise until the solution became clear. The temperature was maintained at ~50°C. The reaction proceeded with stirring at 50°C overnight. The reaction product was then transferred into a dialysis tube (Standard RC Tubing 6-8 kDa, 15370752, Spectrum Laboratories) and dialyzed seven to ten times at 50°C. The PVA-MA solution obtained was then lyophilized to obtain PVA-MA powder. Prefabrication solution was prepared by reconstituting PEG, PVA-MA and LAP in PBS to a final concentration of 10%, 5% and 0.5%, respectively. The solution was then ready for use and was stored in the dark at −20°C. Prefabrication solution was hardened by using a patterned UV irradiation device in all experiments.

Activation of hydrogel and protein binding
The carboxyl groups of the prepared hydrogels were activated by incubating the hydrogel with 10 mg/ml each of NHS/EDC in MES solution at 37°C for 2 h. The solution was replaced with Laminin 511 E8 fragment (Imatrix511, T304, TAKARA BIO) solution (30 µl in 1 ml of PBS) incubated at 37°C

overnight. The next day, the hydrogel was washed three times with PBS and used for cell culture following a standard protocol.

Fluorescent diffusion test

Hydrogels were prepared as described previously. They were then incubated with solutions of fluorescent molecules in PBS for 8 h. Cross-sectional z-stack photos of gels were taken using a fluorescence inverted microscope (SP8 LIGHTNING Confocal Microscope, Leica) and the fluorescence intensity was quantified using LAS X (version 1.4.5 27713, Leica). Details regarding the fluorescent molecules used can be found in Table S3.

Cell culture

The human embryonic stem cell line, KhES-1, was originally established by Kyoto University and is routinely maintained, authenticated and tested for contamination in our laboratory (Suemori et al., 2006). All cells used in this research are below passage number 50. KhES-1 was cultured under feeder-free conditions using StemFit AK02N (RCAK02N, TAKARA BIO) with daily medium change. Cells were routinely passaged every week. On passage day, cells were washed in PBS twice and digested using 50% CTS TrypLE Select Enzyme (Thermo Fisher Scientific, A1285901) at 37°C for 5 min. CTS TrypLE Select Enzyme was then replaced with 2 ml PBS. Cells were collected by gently pipetting and centrifuging at 600 g for 5 min. ROCK Inhibitor Y-27632 (72302, STEMCELL Technologies) (10 µM) was added during passage to improve survival and removed the next day. Laminin 511 E8 fragment (T304, TAKARA BIO) (2.5 µg/ml) was added into the medium during passage as the cell culture matrix. The use of the KhES-1 cell line is approved and performed in accordance with the human embryonic stem cell (ESC) guidelines of the Japanese government.

Generation of H2B-mCherry cell line

PiggyBac donor vector containing H2B fusion mCherry-IRES-puromycin resistant gene under a CAG promoter, PB-CAG-H2B-mCherry-IPuroR, was generated. pCMV-hyPBase was a kind gift from Dr Yusa (Kyoto University, Japan) (Yusa et al., 2011). PB-CAG-H2B-mCherry-IPuroR and pCMV-hyPBase were co-transfected into KhES-1 using Fugene 6 (Promega, E269A) transfection reagent following the manufacturer's instruction. Three days after transfection, 1 µg/ml of puromycin was added to the culture medium to eradicate non-integrated cells. Single colonies with a strong H2B-mCherry fluorescence signal were picked and expanded.

Generation of T-H2B-tdTomato Knock in cell line

T-2A-EGFP-PGK-Puro was a gift from James Thomson (Addgene 83344). T-2A-H2B-tdTomato was generated by replacing the EGFP fragment with H2B-tdTomato using the In-Fusion HD Cloning Kit (639648, Takara), following the manufacturer's instructions, and then linearized using PCR.

A Cas9 and sgRNA all-in-one vector, containing the sgRNA sequence ACCTTCCATGTGAAGCAGCA targeting the 3′ end of the T gene, was generated using the GeneArt CRISPR Nuclease Vector Kit (A21174, ThermoFisher Scientific). The linear donor was then co-transfected with the Cas9 and sgRNA all-in-one vector into KhES-1 cells using the Neon Transfection System 100 µl Kit (MPK10025, ThermoFisher Scientific) following the manufacturer's instructions.

Three days after transfection, 1 µg/ml of puromycin was added to the culture medium to eliminate non-integrated cells. Single colonies were picked and expanded, and stock was frozen at this stage. Colonies were then differentiated using 10 µM CHIR-99021 (72052, STEMCELL Technologies) for 24 h. Colonies showing co-expression of tdTomato and T were used for subsequent experiments.

Genomic PCR was employed to detect integration. The 3′ and 5′ junctions of the HDR site in integrated colonies were further confirmed by Sanger sequencing. The puromycin resistance cassette was subsequently removed from the genome by transfecting a vector containing CRE recombinase. A single colony with puromycin resistance was picked, expanded and used for subsequent experiments. Oligonucleotides used can be found in Table S1.

Interdivision time analysis

To compare the proliferation rate of cells cultured on gel and glass, soft or hard gel coated dish was generated following the previously described protocol. H2B-EGFP cells (1.5×10^5) were seeded into each dish and cultured following the standard protocol. Time-lapse was performed using Olympus LCV100 confocal live imaging system with an interval of 15 min/frame for 72 h. Cells inside similar size colonies on gel or glass from three dishes were manually tracked for interdivision time analysis. The time between each nuclei division was measured according to 15 min/frame, the interdivision time of each cell was tracked at least three times, and the mean value was recorded.

Cell culture on hydrogel

Glass bottom dishes (3961-035, AGC TECHNO) were coated using Bindsilane (10600047, GE Healthcare) following the manufacturer's instruction to improve hydrogel binding. Dishes were then coated with MPC polymer (Lipidure-CM5206, NOR Corporation) to avoid attachment of cells on the non-gel part of the dish, following manufacturer instructions. The prefabrication solution was thawed and briefly vortexed. A prefabrication solution (20 µl) was added to one dish. Cover glass coated with Sigmacote (SL2-25ML, Sigma-Aldrich) was gently put on the gel while avoiding generating bubbles to create a flat gel surface. The gel was then hardened using Desktop Maskless Lithography System (DDB-701-DL, NEOARK CORPORATION). For all experiments, hard gel was hardened with 100% output power UV for 10 s, and soft gel was hardened using 25% output power for 5 s. After gelation, the cover glass was gently removed, and then hydrogel was activated and functionalized using the Laminin511 E8 fragment. Cells were seeded following standard protocol. The culture medium was half replaced on the next day of passage and all media were replaced 2 days after passage to gradually remove Y-27632 to avoid detachment of cells. Cells were then maintained following a standard medium change schedule.

Stiffness measurement of hydrogels using atomic force microscope

In this research, stiffness was exclusively represented by the elastic moduli. The Young's modulus of all hydrogels was measured using an atomic force microscope (AFM) (NanoWizard III, BRUKER). To briefly explain, a tipless cantilever (TL-Cont) with a spring constant of 0.02 N/m and a 10 µm diameter bead attached to the tip were employed for subsequent measurements. These measurements were conducted in the Force Spectroscopy mode within a water medium. The elastic moduli presented here are Young's moduli, determined by applying the Hertz model to force curves. Specifically, only the initial 500 nm of indentation was considered for fitting the force curves. After noise removal using NanoWizard software (V7, BRUKER), Young's modulus was calculated and analyzed with JPKSPM Data Processing software (version 4.2.1, JPK Instruments).

Micropatterned culture on gel

In patterning culture, cells should be seeded at high density as they are cultured on top of the hydrogel patterns. Therefore, the cell seeding area was limited using a PDMS spacer. First, PDMS sheets were prepared by mixing the main agent:hardener (9:1) for 15 min, and then poured onto a flat surface and cured by heating at 80°C for 15-20 min. The sheet was made as thin as possible for subsequent patterning culture. A hole of 6 mm in diameter was made in the center of the formed PDMS sheet using a hole punch. A PDMS spacer was attached to Bindsilane-coated 35 mm glass-bottom dish and 20 µl of PVA-PEG prefabrication solution was added into the hole. A Sigmacote-coated coverslip was then gently put on top of the gel solution. The patterned gel was then cured by irradiating patterned UV using Desktop Maskless Lithography System (DDB-701-DL, NEOARK). Gels with different stiffnesses were generated using spatially different UV exposure (100% output for 10 s for the hard part and 25% output for 5 s for the soft part). The coverslip was then removed, and hydrogel was activated and functionalized with Laminin511 E8 fragment. hESCs (KhES-1) (1×10^6) were collected and resuspended in 200 µl of AK02N medium with 10 µM Y27632.The suspension (200 µl) was added on top of the gel pattern and

incubated at 37°C under 5% CO_2 for 30 min to allow cells to attach. The gel was washed with PBS once to remove excess cells and the PDMS spacer was removed. AK02N medium (1 ml) with 10 μM Y27632 was added to the dish. Half of the medium was replaced with AK02N the next day. Cells were then cultured following standard protocol.

Mesoderm differentiation

Mesoderm differentiation was carried out by following a previously reported method (Evseenko et al., 2010). Shortly, hESCs cultured on gel pattern was generated following the protocol mentioned above. Cell culture medium was replaced with Stemline II Hematopoietic Stem Cell Expansion Medium (S0192-500ML, Sigma-Aldrich) or AK02N (for pulse differentiation) supplemented with 10 ng/ml each of BMP4 (H4916, Sigma-Aldrich) and bFGF (100-18B-1MG, ThermoFisher Scientific) for 24 h.

Live imaging of T-H2B-tdTomato

We generated a patterned culture on a gel with an oval shape, where half of it was soft and the other half was hard, as previously described. In brief, T-H2B-tdTomato cells cultured on the gel pattern, which had locally different stiffness, were subjected to differentiation using either 10 μM CHIR or 10 ng/ml each of BMP4 and bFGF for 24 h. Subsequently, the differentiating medium was removed, and the samples were washed twice with PBS before being returned to the maintenance culture medium.

In YAP inhibition experiments, the cells were pretreated with Peptide 17 (S8164, Selleck Chemicals) for 6 h before they were differentiated with 10 ng/ml each of BMP4 and bFGF under the presence of Peptide 17. After differentiation, the cells were subjected to live imaging. For imaging of T expression, we used the Olympus LCV100 confocal live imaging system, capturing images at intervals of 60 min per frame for a duration of 48 h.

Measuring protein binding ability of PVA-MA

PVA-MA hydrogel was prepared and activated as described previously. The hydrogel was then incubated with a fluorescent 2nd antibody (A-11003, ThermoFisher Scientific) following the protein binding protocol described previously. Z stack photos of the gel surface were taken using a fluorescence inverted microscope (SP8 LIGHTNING Confocal Microscope, Leica) and the fluorescence intensity was quantified using LAS X(V 1.4.5 27713, Leica).

Immunofluorescence

The culture medium was removed from the sample. Samples were then fixed by incubating in 2 ml of 4% PFA in PBS on ice for 20 min. Samples were washed in PBS three times for 5 min each. PBS was replaced with 0.3% Triton-X100/PBS and samples were incubated for 5 min at 25°C. Samples were then blocked with Blocking One (03953-66, NACALAI TESQUE) for 1 h at room temperature, then incubated with primary antibody diluted in blocking one at 4°C overnight. Primary antibody was removed, then samples were washed with 0.05% Tween 20/PBS for 5 min and repeated three times. Then samples were incubated with secondary antibodies and DAPI diluted in the blocking solution, 1/500 for 1 h at room temperature. Secondary antibodies were removed, and samples were washed in 0.05% Tween 20/PBS for 5 min three times. The samples were then observed using a microscope. Antibodies used can be found in Table S2.

RNA extraction and quantitative PCR

Total RNA was extracted using RNeasy Mini Kit (74106, QIAGEN) following the manufacturer's instructions. cDNA was reverse transcribed from 500 ng RNA using PrimeScript II 1st strand cDNA Synthesis Kit (6210A TAKARA BIO) following the manufacturer's instructions. qPCR was performed using Power SYBR Green Master Mix (4368577, Applied Biosystems). The expression level of mRNAs was calculated and normalized based on indicated housekeeping gene [*HPRT1* or *PBGD* (*HMBS*)].

RNA-seq

Gel-coated 35 mm glass-bottom dishes were prepared as previously described. KhES-1 was seeded on the soft gel, hard gel or uncoated glass-bottom dish, and cultured for 4 days before they were collected as previously described. Total RNA was extracted using RNeasy Mini Kit (74106, Qiagen) following the manufacturer's instructions. Two samples for each group, six samples in total, were collected. Libraries were prepared from 100 ng of total RNA using the following kits, NEBNext Poly(A) mRNA Magnetic Isolation Module (E7490, New England Biolabs), NEBNext Ultra II Directional RNA Library Prep Kit (E7760, New England Biolabs), NEBNext Multiplex Oligos for Illumina (96 Unique Dual Index Primer Pairs) (E6440, New England Biolabs) following the manufacturer's instructions. Sequencing was performed with the paired-end mode (more than 50 bp at both ends) to have at least 15 clusters per sample using the NextSeq550 NGS system.

The raw RNA-seq files generated were quality controlled using FastQC version 0.11.8 and Trimomatic version 0.39. High-quality sequence reads were then mapped and annotated with STAR version 2.7.6a against the GRCh38 reference genome. Subsequently, count data were estimated using subread version 2.0.1 and subjected to differential gene expression analysis using the Bioconductor package DESeq2 version 1.30.1 in R version 4.0.3. Differentially expressed genes (DEGs) were defined as genes with a false discovery rate (FDR)<0.1. The Metascape database platform was used to enrich and analyze Gene Ontology (GO) annotations. For the TPM matrix, RSEM version 1.3.3 was used to quantify data from STAR-mapped reads (Li and Dewey, 2011).

YAP quantification

Nucleocytoplasmic transport of YAP was quantified using the N/C intensity ratio (Kelley and Paschal, 2019). In brief, cells cultured on hard and soft gels or on a rigid dish were subjected to immunofluorescence staining following the previously mentioned protocol. Z-stack images were acquired, and a z-projection was generated using the Sum Slices method in ImageJ2 (Rueden et al., 2017). To mitigate the impact of confluency on YAP localization, we focused on quantifying small colonies containing fewer than 20 cells.

In summary, the process involved thresholding a DAPI image for nuclear staining to create a mask defining the nuclear area. Simultaneously, the YAP-stained channel was thresholded to delineate the cytoplasmic area containing the nuclear region. The nuclear area was then subtracted from the YAP-stained image using the DAPI-generated mask. The resulting area was used to measure the total fluorescence intensity of the cytoplasm. The nuclear/cytoplasmic (N/C) ratio was calculated as follows: N/C=total intensity of the nucleus/total intensity of the cytoplasm.

Manuscript preparation

ChatGPT (version 3.5, Open AI, San Francisco, CA, USA) was used to check and improve the clarity and grammar of written manuscript. After using this service, the authors reviewed and edited the content as needed, and take full responsibility for the content of the publication.

Statistical analysis

Statistical analysis was carried out using GraphPad Prism (version 9.3.1, GraphPad Software). Two-tailed unpaired *t*-test was used to compare the differences between the two groups. All data were derived from a minimum of three biological replicates.

Competing interests
The authors declare no competing or financial interests.

Author contributions
Conceptualization: Z.W., A.N., M.E.; Methodology: Z.W., A.N., M.E.; Software: Z.W., Y.O., F.W.; Validation: Z.W.; Formal analysis: Z.W.; Investigation: Z.W., A.N.; Resources: Z.W., M.O.; Data curation: Z.W., A.N., K.M.; Writing - original draft: Z.W.;

Data availability
RNA-seq data have been deposited in SRA under accession number PRJNA1022777.

Peer review history
The peer review history is available online at https://journals.biologists.com/dev/lookup/doi/10.1242/dev.201621.reviewer-comments.pdf

References
Candiello, J., Singh, S. S., Task, K., Kumta, P. N. and Banerjee, I. (2013). Early differentiation patterning of mouse embryonic stem cells in response to variations in alginate substrate stiffness. *J. Biol. Eng.* **7**, 9. doi:10.1186/1754-1611-7-9

Chambers, S. M., Fasano, C. A., Papapetrou, E. P., Tomishima, M., Sadelain, M. and Studer, L. (2009). Highly efficient neural conversion of human ES and iPS cells by dual inhibition of SMAD signaling. *Nat. Biotechnol.* **27**, 275-280. doi:10.1038/nbt.1529

Chen, G., Tang, W., Wang, X., Zhao, X., Chen, C. and Zhu, Z. (2019). Applications of hydrogels with special physical properties in biomedicine. *Polymers (Basel)* **11**, 1420. doi:10.3390/polym11091420

Chen, Y. F., Li, Y. J., Chou, C. H., Chiew, M. Y., Huang, H. D., Ho, J. H., Chien, S. and Lee, O. K. (2020). Control of matrix stiffness promotes endodermal lineage specification by regulating SMAD2/3 via lncRNA LINC00458. *Sci. Adv.* **6**, eaay0264.

D'Amour, K. A., Agulnick, A. D., Eliazer, S., Kelly, O. G., Kroon, E. and Baetge, E. E. (2005). Efficient differentiation of human embryonic stem cells to definitive endoderm. *Nat. Biotechnol.* **23**, 1534-1541. doi:10.1038/nbt1163

Estaras, C., Hsu, H. T., Huang, L. and Jones, K. A. (2017). YAP repression of the WNT3 gene controls hESC differentiation along the cardiac mesoderm lineage. *Genes Dev.* **31**, 2250-2263. doi:10.1101/gad.307512.117

Evseenko, D., Zhu, Y., Schenke-Layland, K., Kuo, J., Latour, B., Ge, S., Scholes, J., David, G., Li, X., MacLellan, W. R. et al. (2010). Mapping the first stages of mesoderm commitment during differentiation of human embryonic stem cells. *Proc. Natl. Acad. Sci. USA* **107**, 13742-13747. doi:10.1073/pnas.1002077107

Gattazzo, F., Urciuolo, A. and Bonaldo, P. (2014). Extracellular matrix: a dynamic microenvironment for stem cell niche. *Biochim. Biophys. Acta* **1840**, 2506-2519. doi:10.1016/j.bbagen.2014.01.010

Guo, A., Wang, B., Lyu, C., Li, W., Wu, Y., Zhu, L., Bi, R., Huang, C., Li, J. J. and Du, Y. (2020). Consistent apparent Young's modulus of human embryonic stem cells and derived cell types stabilized by substrate stiffness regulation promotes lineage specificity maintenance. *Cell Regen.* **9**, 15. doi:10.1186/s13619-020-00054-4

Hsu, H.-T., Estarás, C., Huang, L. and Jones, K. A. (2018). Specifying the anterior primitive streak by modulating YAP1 levels in human pluripotent stem cells. *Stem Cell Rep.* **11**, 1357-1364. doi:10.1016/j.stemcr.2018.10.013

Karzbrun, E., Khankhel, A. H., Megale, H. C., Glasauer, S. M. K., Wyle, Y., Britton, G., Warmflash, A., Kosik, K. S., Siggia, E. D., Shraiman, B. I. et al. (2021). Human neural tube morphogenesis in vitro by geometric constraints. *Nature* **599**, 268-272. doi:10.1038/s41586-021-04026-9

Kechagia, Z., Saez, P., Gomez-Gonzalez, M., Canales, B., Viswanadha, S., Zamarbide, M., Andreu, I., Koorman, T., Beedle, A. E. M., Elosegui-Artola, A. et al. (2023). The laminin-keratin link shields the nucleus from mechanical deformation and signalling. *Nat. Mater.* **22**, 1409-1420. doi:10.1038/s41563-023-01657-3

Kelley, J. B. and Paschal, B. M. (2019). Fluorescence-based quantification of nucleocytoplasmic transport. *Methods* **157**, 106-114. doi:10.1016/j.ymeth.2018.11.002

Kempf, H., Olmer, R., Haase, A., Franke, A., Bolesani, E., Schwanke, K., Robles-Diaz, D., Coffee, M., Gohring, G., Drager, G. et al. (2016). Bulk cell density and Wnt/TGFbeta signalling regulate mesendodermal patterning of human pluripotent stem cells. *Nat. Commun.* **7**, 13602. doi:10.1038/ncomms13602

Keung, A. J., Asuri, P., Kumar, S. and Schaffer, D. V. (2012). Soft microenvironments promote the early neurogenic differentiation but not self-renewal of human pluripotent stem cells. *Integr. Biol.* **4**, 1049-1058. doi:10.1039/c2ib20083j

Kumbar, S. G., James, R., Nukavarapu, S. P. and Laurencin, C. T. (2008). Electrospun nanofiber scaffolds: engineering soft tissues. *Biomed. Mater.* **3**, 034002. doi:10.1088/1748-6041/3/3/034002

Lee, S., Tong, X. and Yang, F. (2014). The effects of varying poly(ethylene glycol) hydrogel crosslinking density and the crosslinking mechanism on protein accumulation in three-dimensional hydrogels. *Acta Biomater.* **10**, 4167-4174. doi:10.1016/j.actbio.2014.05.023

Lee, S., Stanton, A. E., Tong, X. and Yang, F. (2019). Hydrogels with enhanced protein conjugation efficiency reveal stiffness-induced YAP localization in stem cells depends on biochemical cues. *Biomaterials* **202**, 26-34. doi:10.1016/j.biomaterials.2019.02.021

Li, B. and Dewey, C. N. (2011). RSEM: accurate transcript quantification from RNA-Seq data with or without a reference genome. *BMC Bioinformatics* **12**, 323. doi:10.1186/1471-2105-12-323

Loh, K. M., Chen, A., Koh, P. W., Deng, T. Z., Sinha, R., Tsai, J. M., Barkal, A. A., Shen, K. Y., Jain, R., Morganti, R. M. et al. (2016). Mapping the pairwise choices leading from pluripotency to human bone, heart, and other mesoderm cell types. *Cell* **166**, 451-467. doi:10.1016/j.cell.2016.06.011

Maldonado, M., Luu, R. J., Ico, G., Ospina, A., Myung, D., Shih, H. P. and Nam, J. (2017). Lineage- and developmental stage-specific mechanomodulation of induced pluripotent stem cell differentiation. *Stem Cell Res. Ther.* **8**, 216. doi:10.1186/s13287-017-0667-2

Martyn, I., Kanno, T. Y., Ruzo, A., Siggia, E. D. and Brivanlou, A. H. (2018). Self-organization of a human organizer by combined Wnt and Nodal signalling. *Nature* **558**, 132-135. doi:10.1038/s41586-018-0150-y

Millar-Haskell, C. S., Dang, A. M. and Gleghorn, J. P. (2019). Coupling synthetic biology and programmable materials to construct complex tissue ecosystems. *MRS Commun.* **9**, 421-432. doi:10.1557/mrc.2019.69

Muduli, S., Chen, L. H., Li, M. P., Heish, Z. W., Liu, C. H., Kumar, S., Alarfaj, A. A., Munusamy, M. A., Benelli, G., Murugan, K. et al. (2017). Stem cell culture on polyvinyl alcohol hydrogels having different elasticity and immobilized with ECM-derived oligopeptides. *J. Polym. Eng.* **37**, 647-660. doi:10.1515/polyeng-2016-0193

Muncie, J. M., Ayad, N. M. E., Lakins, J. N., Xue, X., Fu, J. and Weaver, V. M. (2020). Mechanical tension promotes formation of gastrulation-like nodes and patterns mesoderm specification in human embryonic stem cells. *Dev. Cell* **55**, 679-694.e11. doi:10.1016/j.devcel.2020.10.015

Musah, S., Wrighton, P. J., Zaltsman, Y., Zhong, X., Zorn, S., Parlato, M. B., Hsiao, C., Palecek, S. P., Chang, Q., Murphy, W. L. et al. (2014). Substratum-induced differentiation of human pluripotent stem cells reveals the coactivator YAP is a potent regulator of neuronal specification. *Proc. Natl. Acad. Sci. USA* **111**, 13805-13810. doi:10.1073/pnas.1415330111

Pagliari, S., Vinarsky, V., Martino, F., Perestrelo, A. R., Oliver De La Cruz, J., Caluori, G., Vrbsky, J., Mozetic, P., Pompeiano, A., Zancla, A. et al. (2021). YAP–TEAD1 control of cytoskeleton dynamics and intracellular tension guides human pluripotent stem cell mesoderm specification. *Cell Death Differ.* **28**, 1193-1207. doi:10.1038/s41418-020-00643-5

Perez-Puyana, V., Jimenez-Rosado, M., Romero, A. and Guerrero, A. (2020). Polymer-based scaffolds for soft-tissue engineering. *Polymers (Basel)* **12**, 1566. doi:10.3390/polym12071566

Przybyla, L., Lakins, J. N. and Weaver, V. M. (2016). Tissue mechanics orchestrate Wnt-dependent human embryonic stem cell differentiation. *Cell Stem Cell* **19**, 462-475. doi:10.1016/j.stem.2016.06.018

Qin, H., Hejna, M., Liu, Y., Percharde, M., Wossidlo, M., Blouin, L., Durruthy-Durruthy, J., Wong, P., Qi, Z., Yu, J. et al. (2016). YAP induces human naive pluripotency. *Cell Rep.* **14**, 2301-2312. doi:10.1016/j.celrep.2016.02.036

Rosowski, K. A., Mertz, A. F., Norcross, S., Dufresne, E. R. and Horsley, V. (2015). Edges of human embryonic stem cell colonies display distinct mechanical properties and differentiation potential. *Sci. Rep.* **5**, 14218. doi:10.1038/srep14218

Rueden, C. T., Schindelin, J., Hiner, M. C., DeZonia, B. E., Walter, A. E., Arena, E. T. and Eliceiri, K. W. (2017). ImageJ2: imageJ for the next generation of scientific image data. *BMC Bioinformatics* **18**, 529. doi:10.1186/s12859-017-1934-z

Shao, Y., Sang, J. and Fu, J. (2015). On human pluripotent stem cell control: the rise of 3D bioengineering and mechanobiology. *Biomaterials* **52**, 26-43. doi:10.1016/j.biomaterials.2015.01.078

Shibata, S., Hayashi, R., Okubo, T., Kudo, Y., Katayama, T., Ishikawa, Y., Toga, J., Yagi, E., Honma, Y., Quantock, A. J. et al. (2018). Selective laminin-directed differentiation of human induced pluripotent stem cells into distinct ocular lineages. *Cell Rep.* **25**, 1668-1679.e1665. doi:10.1016/j.celrep.2018.10.032

Simunovic, M. and Brivanlou, A. H. (2017). Embryos, organoids and gastruloids: new approaches to understanding embryogenesis. *Development* **144**, 976-985. doi:10.1242/dev.143529

Smith, Q., Rochman, N., Carmo, A. M., Vig, D., Chan, X. Y., Sun, S. and Gerecht, S. (2018). Cytoskeletal tension regulates mesodermal spatial organization and subsequent vascular fate. *Proc. Natl. Acad. Sci. USA* **115**, 8167-8172. doi:10.1073/pnas.1808021115

Srivastava, P., Romanazzo, S., Kopecky, C., Nemec, S., Ireland, J., Molley, T. G., Lin, K., Jayathilaka, P. B., Pandzic, E., Yeola, A. et al. (2023). Defined

microenvironments trigger in vitro gastrulation in human pluripotent stem cells. *Adv. Sci.* **10**, e2203614. doi:10.1002/advs.202203614

Stanton, A. E., Tong, X., Lee, S. and Yang, F. (2019). Biochemical ligand density regulates yes-associated protein translocation in stem cells through cytoskeletal tension and integrins. *ACS Appl. Mater. Interfaces* **11**, 8849-8857. doi:10.1021/acsami.8b21270

Stronati, E., Giraldez, S., Huang, L., Abraham, E., McGuire, G. R., Hsu, H. T., Jones, K. A. and Estaras, C. (2022). YAP1 regulates the self-organized fate patterning of hESC-derived gastruloids. *Stem Cell Rep.* **17**, 211-220. doi:10.1016/j.stemcr.2021.12.012

Suemori, H., Yasuchika, K., Hasegawa, K., Fujioka, T., Tsuneyoshi, N. and Nakatsuji, N. (2006). Efficient establishment of human embryonic stem cell lines and long-term maintenance with stable karyotype by enzymatic bulk passage. *Biochem. Biophys. Res. Commun.* **345**, 926-932. doi:10.1016/j.bbrc.2006.04.135

Surmacz, B., Fox, H., Gutteridge, A., Fish, P., Lubitz, S. and Whiting, P. (2012). Directing differentiation of human embryonic stem cells toward anterior neural ectoderm using small molecules. *Stem Cells* **30**, 1875-1884. doi:10.1002/stem.1166

Tibbitt, M. W. and Anseth, K. S. (2009). Hydrogels as extracellular matrix mimics for 3D cell culture. *Biotechnol. Bioeng.* **103**, 655-663. doi:10.1002/bit.22361

Virdi, J. K. and Pethe, P. (2021). Biomaterials regulate mechanosensors YAP/TAZ in stem cell growth and differentiation. *J. Tissue Eng. Regen. Med.* **18**, 199-215. doi:10.1007/s13770-020-00301-4

Wang, H., Luo, X. and Leighton, J. (2015). Extracellular matrix and integrins in embryonic stem cell differentiation. *Biochem. Insights* **8**, 15-21. doi:10.4137/BCI.S30377

Warmflash, A., Sorre, B., Etoc, F., Siggia, E. D. and Brivanlou, A. H. (2014). A method to recapitulate early embryonic spatial patterning in human embryonic stem cells. *Nat. Methods* **11**, 847-854. doi:10.1038/nmeth.3016

Yusa, K., Zhou, L. Q., Li, M. A., Bradley, A. and Craig, N. L. (2011). A hyperactive piggyBac transposase for mammalian applications. *Proc. Natl. Acad. Sci. USA* **108**, 1531-1536. doi:10.1073/pnas.1008322108

Zhang, D. W., Yang, S. Z., Toledo, E. M., Gyllborg, D., Salto, C., Villaescusa, J. C. and Arenas, E. (2017). Niche-derived laminin-511 promotes midbrain dopaminergic neuron survival and differentiation through YAP. *Sci. Signal.* **10**, eaal4165. doi:10.1126/scisignal.aal4165

DEVELOPMENT